IEEE Photonics Journal
An IEEE Photonics Society Publication

Open Access

Large-Range, Highly-Sensitive, and Fast-Responsive Optical Fiber Temperature Sensor Based on the Sealed Ethanol in Liquid State Up to its Supercritical Temperature

Volume 11, Number 6, December 2019

Yingying Liao
Yi Liu
Yan Li
Changpeng Lang
Kunjian Cao
Shiliang Qu

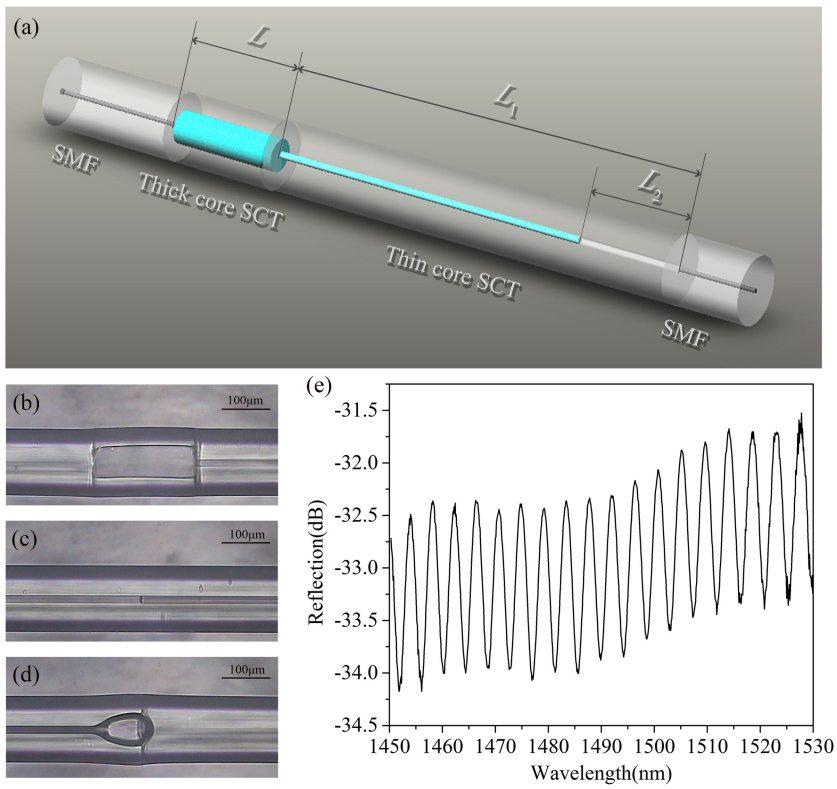

DOI: 10.1109/JPHOT.2019.2946284

Large-Range, Highly-Sensitive, and Fast-Responsive Optical Fiber Temperature Sensor Based on the Sealed Ethanol in Liquid State Up to its Supercritical Temperature

Yingying Liao,[1] Yi Liu,[1] Yan Li,[1] Changpeng Lang,[1,2] Kunjian Cao,[1] and Shiliang Qu[2]

[1]Department of Optoelectronics Science, Harbin Institute of Technology at Weihai, Weihai 264209, China
[2]Department of Physics, Harbin Institute of Technology, Harbin 150001, China

DOI:10.1109/JPHOT.2019.2946284

Manuscript received July 21, 2019; revised September 27, 2019; accepted October 3, 2019. Date of publication October 10, 2019; date of current version October 23, 2019. This work was supported in part by the National Natural Science Foundation of China (NSFC) under Grants 11874133, 11574063, and 11874010, in part by Natural Science Foundation of Shandong Province under Grant ZR2018MF031, and in part by the Science and Technology Development Plan of Weihai under Grant 2015DXGJUS002.
Corresponding author: Yi Liu (e-mail: shandongliu2006@163.com).

Abstract: A highly-sensitive and fast-responsive optical fiber temperature sensor based on the sealed liquid ethanol with a large detection range was proposed. The ethanol was injected into the fiber Fabry-Perot (FP) micro-cavity through the thin core silica capillary tube (SCT), which was then spliced to a section of singe mode fiber. A section of air core was formed in the thin core SCT near the splicing position. If the volume of the sealed ethanol is much larger than that of the air core, the ethanol can remain liquid state until its supercritical temperature (about 243 °C) at which the ethanol becomes supercritical state. The temperature sensitivity of proposed sensor with a volume ratio 2.89 of ethanol to air reaches –497.6 pm/ °C with an upper detection limit of 220 °C. Meanwhile, the order of the interference fringe can be distinguished by monitoring the transmission loss of the sensor, which can assist wavelength demodulation in the large detection range. Besides, the proposed fiber temperature sensor is with the advantages of fast response (less than 1 s for the temperature variation of about 90 °C) and good repeatability.

Index Terms: Optical fiber sensor, temperature, liquid ethanol, interferometry.

1. Introduction

In recent years, optical fiber temperature sensors have attracted increasing attention owing to their compact structure, fast response, real-time sensing and immunity to electromagnetic interference. Different optic fiber structures, such as fiber Bragg grating (FBG) [1], long-period fiber grating (LPG) [2], Mach-Zehnder interferometer (MZI) [3], [4], and Fabry-Perot interferometer (FPI) [5], [6], have been reported to be applied for temperature sensing. However, the temperature sensitivities of these fiber sensors are not high enough due to the low thermo-optical coefficient (TOC) and thermal expansion coefficient (TEC) of silica material. To enhance the sensitivities of optical fiber temperature sensors, kinds of solid polymer materials were combined with the optical fiber

sensing structures, and their sensitivities reached about 300∼500 pm/ °C. However, there is a common problem to these sensors based on the solid material, whether silica or polymer. That is the existence of the thermal stress and thermal nonequilibrium in the solid material [7] during the sensor fabrication process, which results in the hysteresis [8]. To reduce the hysteresis, a suitable high-temperature annealing for several hours is needed [7]. Besides, the sensors based on the solid material exhibit slow temperature response in the environment with rapid and large range temperature variation. For example, the reported fiber sensors based on the FBGs were with the response time of about 10 s during the temperature variation range of 100 °C [9], and the fiber sensors based on the polymer with smaller response time was still about 13 s during the temperature variation range of 200 °C [10]. For the thermal stress has nearly no influence on the liquid, the liquid materials with higher TOC and TEC were integrated into the optical fiber sensors by immerging the fiber structure in the liquid [11], [12] or filling the liquid such as liquid crystal [13], toluene [14], glycerol [15] and ethanol [16] into the fiber structure. These sensors are with good repeatability in temperature increasing and decreasing processes [17], [18] without extra annealing treatment. Besides, for the liquid materials are with higher TOC and TEC, their sensitivities range from 300 pm/ °C to 10 nm/ °C depending on the different mechanisms of the sensing structures [19], [20]. Among these liquid materials, ethanol was most popular owing to its non-toxicity and low viscosity [21]–[27]. However, as the boiling point of the ethanol in common environment is only about 78 °C, the reported optical fiber sensors based on the ethanol were tested under the temperature only less than 70 °C [21]–[27], which resulted in a small temperature detection range.

In this paper, we proposed a highly-sensitive and fast-responsive optical fiber temperature sensor based on the sealed liquid ethanol with a large detection range (up to 220 °C). A section of thick core silica capillary tube (SCT) with an internal diameter of 60 μm and an external diameter of 125 μm was spliced between a single mode fiber (SMF) and a thin core SCT with an internal diameter of 13 μm and an external diameter of 125 μm to form a fiber inline Fabry-Perot (FP) micro-cavity. The ethanol was injected into the FP micro-cavity through the thin core SCT. Then the thin core SCT was spliced to another section of SMF to seal the ethanol into the fiber structure. A section of air core was formed in the thin core SCT near the splicing position due to the arc discharging in the fiber splicing process. The experimental results show that if the volume of the ethanol is much larger than that of the air core, the sealed ethanol can remain liquid state as the increasing of the temperature until its supercritical temperature (about 243 °C) at which the ethanol becomes supercritical state. In this process, the whole structure will not burst along with the rapid increasing of the ethanol pressure owing to the advantage of the ethanol sealing method, and the refractive index (RI) of the ethanol decreased linearly until the air core area was also completely filled by the ethanol. Then the RI of the ethanol remained almost unchanged as the further increasing of the temperature. Based on the wavelength shift of the interference fringe induced by the RI variation of the ethanol in the FP micro-cavity, the temperature sensitivity of the proposed sensor with a volume ratio 2.89 of ethanol to air reached –497.6 pm/ °C until the temperature reached 220 °C. Meanwhile, the temperature cycle experiment results show the good repeatability of the proposed sensor, and the response time of the proposed sensor is much better than other reported fiber temperature sensors based on the solid materials [9], [10]. Besides, the order of the interference fringe can be distinguished by monitoring the transmission loss of the sensor, which can help to achieve the accurate wavelength demodulation in a large temperature variation range when the shift of the interference fringe exceeds one free spectrum range (FSR).

2. Fabrication

The fabrication process of the proposed fiber temperature sensor based on the sealed ethanol is shown in Fig. 1. In the First step, as shown in Fig. 1(a), a section of thick core SCT with an outer diameter of 125 μm and an inner diameter of 60 μm was spliced with a cleaved single mode fiber (SMF) by using a commercial fusion splicer and then the SCT was cleaved at a desired length *L*. Another section of thin core SCT with an outer diameter of 125 μm and an inner diameter of 13 μm was connected with a syringe filled by the ethanol. In the second step, the two sections of SCTs

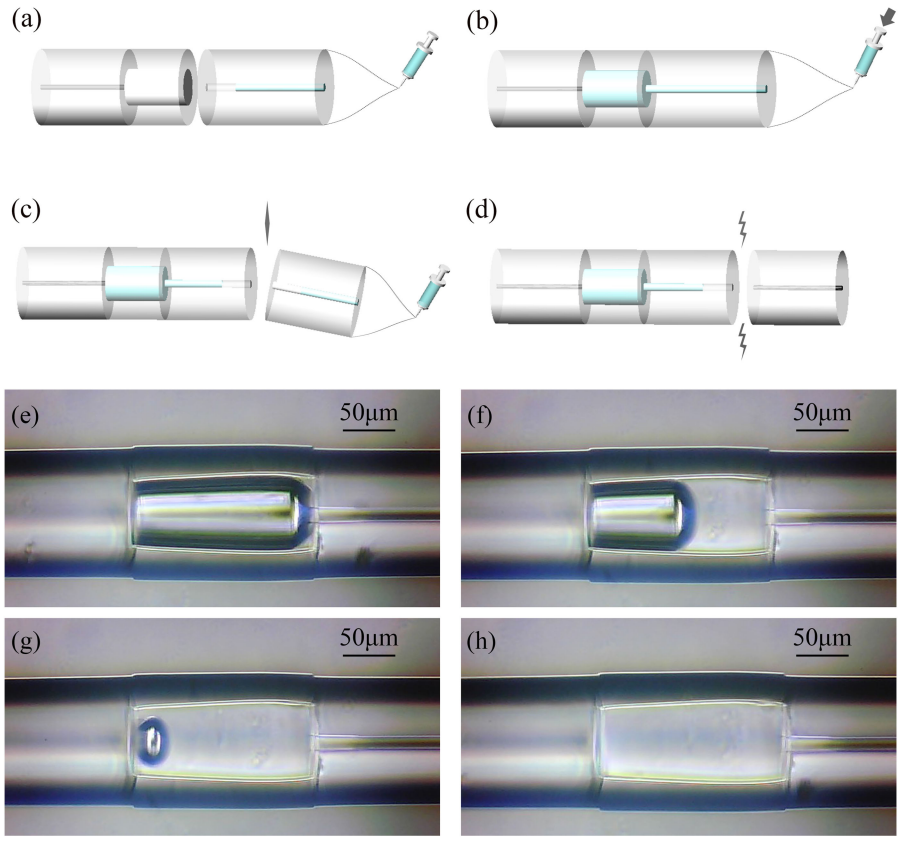

Fig. 1. (a)–(d) Fabrication process diagram of the proposed fiber sensor based on the sealed ethanol. (e)–(h) Ethanol filling processes by using the thin core SCT and the syringe.

were spliced together to form a micro-cavity at the thick core SCT position. Ethanol was then slowly injected into the micro-cavity through the thin core SCT, which is shown in Fig. 1(b). In this step, the spliced structure was kept in the fusion splicer, and the ethanol filled in the micro-cavity can be seen through the display screen of the fusion splicer. In the third step, as shown in Fig. 1(c), after the micro-cavity was fully filled by the ethanol, the thin core SCT was cleaved at a desired length L_1. In this process, part of the ethanol at the end of the thin core SCT evaporated because of its high volatility. In the final step, the thin core SCT was spliced with another SMF to seal the ethanol in the fiber structure as show in Fig. 1(d).

It should be noted that, if one side of the thick core SCT is spliced to the SMF and the other side is connected with the syringe directly, it is very difficult to fully fill the thick core SCT due to the presence of air with a large volume in the thick core SCT. Here, the thin core SCT was partly filled by the ethanol, and then spliced to the thick core SCT. This process is crucial, for the volume of the air left in the SCT before compression was reduced greatly in advance. Then as the pressure increasing of the syringe, the air in the cavity (thick core SCT) was compressed, and the ethanol reached the splicing interface between the thick core SCT and the thin core SCT. For the inner diameter of the thick core SCT was much larger than that of the thin core SCT, the ethanol flowed along the in-wall of the cavity as shown in Fig. 1(e). Then as the further increasing of the syringe pressure, the air in the cavity was further compressed as shown in Fig. 1(f). Gradually, the air was surrounded by the ethanol and formed an air-bubble in the cavity as shown in Fig. 1(g). The volume of the air-bubble decreased along with the increasing of the pressure. Finally, the air molecules in the bubble were integrated into the liquid ethanol molecules because of high pressure, and the

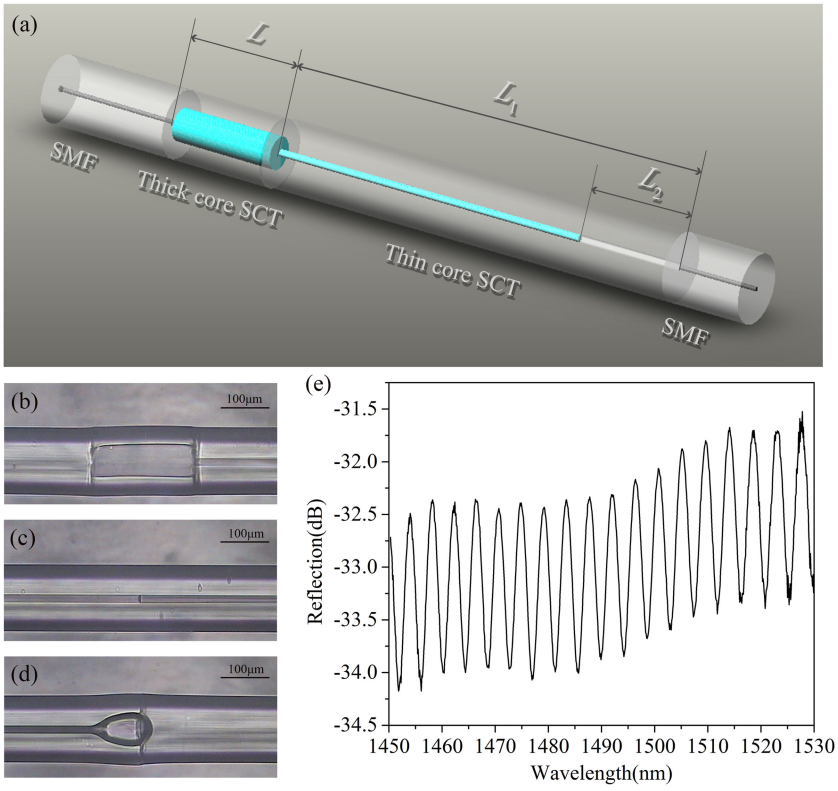

Fig. 2. (a) Structural diagram of the proposed fiber temperature sensor. (b) Microscope image of the micro-cavity section. (c) Interface between the ethanol and air. (d) Interface between the thin core SCT and SMF. (e) Corresponding reflection spectra of the fiber temperature sensor.

air-bubble disappeared as shown in Fig. 1(h). In this way, the cavity was fully filled by the liquid ethanol.

The final diagram of the fabricated fiber structure is shown in Fig. 2(a). The micro-cavity formed by the thick core SCT with a length of L is fully filled by the ethanol. When the thin core SCT was spliced with another SMF, more ethanol at the end of the thin core SCT was gasified instantaneously by the arc discharging. Therefore, a section of air column with a length of L_2 was formed at the end of the thin core SCT after fiber fusion splicing, and the length of the left ethanol in the thin core SCT was L_1–L_2. The existence of the air column was not conducive to improving the boiling point of the ethanol. But it was inevitable by using the proposed fiber fusion splicing method. Of course, the liquid can be sealed in the SCT by using curing adhesive without leaving a section of air column [28]. However, the fiber structure sealed by the curing adhesive cannot survive under ultrahigh pressure, and it may burst along with the rapid expansion of the liquid induced by the increasing of the temperature. The fiber fusion splicing method to seal the ethanol in the SCT can solve this problem and avoid the leakage of the ethanol under high temperature. Besides, the air column in the thin core SCT provides the space for the thermal expansion of the ethanol, which makes sure that the RI of the ethanol in the FP cavity can decrease obviously along with the increasing of the temperature. After repeated tests, to achieve good mechanical property at the splicing point, the heating current and heating time of the fiber fusion splicer were set to be 1.6 mA and 600 ms respectively, and the length L_2 of the air column was about 2 mm.

Though the existence of the air column was inevitable, the micro-cavity formed by the thick core SCT can help to increase the volume ratio of ethanol to air greatly, for the inner diameter of the thick core SCT is much larger than that of the thin core SCT, and this volume ratio value can be further improved by increasing the values of L and L_1. The high ratio value of ethanol to air and stable

sealing space result in the elevation of boiling point of the ethanol, and the ethanol can remain liquid state in the proposed fiber structure even under high temperature. However, the ratio value of ethanol to air cannot be too large. If the volume of the air core is too small, the expansion of the ethanol will be limited. As a result, the RI of the ethanol in the FP cavity will be not sensitive enough to the variation of the temperature, which will seriously influence the temperature sensitivity value of the sensor.

Fig. 2(b)–2(d) are the actual microscope images of one of the fabricated fiber structures, and the volume ratio of ethanol to air was about 2.89. The micro-cavity formed by the thick core SCT is shown in Fig. 2(b), and its length L is about 200 μm. We can see that the ethanol has completely filled the micro-cavity. The length of liquid and air in thin core SCT is about 1460 μm and 1980 μm, respectively. The interface between liquid and air in thin core SCT is shown in Fig. 2(c). The liquid is on the left, and the air is on the right. The splicing interface between the thin core SCT and SMF is shown in Fig. 2(d). There is a micro-bubble at the splicing position due to the expansion of the gaseous ethanol. The reflection spectrum of the fabricated fiber structure was measured by using an optical spectrum analyzer (OSA) (YOKOGAWA, AQ6370B) and a broadband light source (BBS) (1200 nm to 1700 nm) through a circulator as shown in Fig. 2(e). The reflection spectrum shows interference fringe which is induced from the interference of the light beams reflected by the two side walls of the micro-cavity shown in Fig. 2(b).

3. Principle

The interface between the SMF and thick core SCT acts as the reflector 1 and the interface between the thick core SCT and the thin core SCT acts as the reflector 2. These two reflectors constitute a two-beam FPI. The total reflected electric field is given by [29]:

$$E_r \approx \sqrt{R_1}\sqrt{1-B_1}E_0 + (1-A_1)(1-\alpha)(1-R_1)\sqrt{R_2}\sqrt{1-B_2}E_0 e^{-j2\gamma L + j\pi} \tag{1}$$

where E_0 is the input field, A_1 is the transmission loss factor at reflector 1, B_1 and B_2 are the reflection loss factors at reflector 1 and reflector 2 respectively, γ is the propagation constant of the guided mode of the fiber, and α is the loss factor of micro-cavity. R_1 and R_2 are the reflectivity of two reflectors, which can be expressed by Fresnel formula:

$$R_1 = \left(\frac{n_1 - n_e}{n_1 + n_e}\right)^2 \tag{2}$$

$$R_2 = \left(\frac{n_e - n_2}{n_e + n_2}\right)^2 \tag{3}$$

where n_1, n_2 and n_e are the RI of fiber core, silica and ethanol filling the cavity respectively. There is a π-phase shift at reflector 2 for light is reflected from an optically denser medium. Based on $R_{FP}(\lambda) = |E_r/E_0|^2$, we obtained the normalized reflection spectrum as follows:

$$\begin{aligned} R_{FP}(\lambda) = {} & R_1(1-B_1) + (1-A_1)^2(1-\alpha)^2(1-R_1)^2 R_2(1-B_1) \\ & + \sqrt{R_1}\sqrt{1-B_1}(1-A_1)(1-\alpha)(1-R_1)\sqrt{R_2}\sqrt{1-B_2}\cos(4\pi jL/\lambda + j\lambda) \end{aligned} \tag{4}$$

As an example, we set $A_1 = 0.45$, $B_1 = 0.5$, $B_2 = 0.8$, $\alpha = 0.75$, $L = 200$ μm, $n_1 = 1.452$, $n_2 = 1.447$, and $n_e = 1.361 + \beta_{TOC}\Delta T$. Here, 1.361 is the RI of the ethanol at 20 °C, and β_{TOC} ($\sim -3.7 \times 10^{-4}$) is the TOC of the ethanol [30]. ΔT is the variation of the temperature. The TEC and TOC of the fiber core and silica material can be negligible. Therefore, along with the variation of the temperature, only the value of n_e changed. Assuming the boiling point of the ethanol can be improved to more than 180 °C, we simulated the reflection spectra of the proposed fiber structure at different temperature and the results are shown in Fig. 3.

From Fig. 3 it can be seen that, as the increasing of the temperature, the interference fringe shifts to the shorter wavelength direction. At the same time, the mean loss of the interference fringe decreases gradually. From Eq. (4), the interference fringe reaches its valley when the following

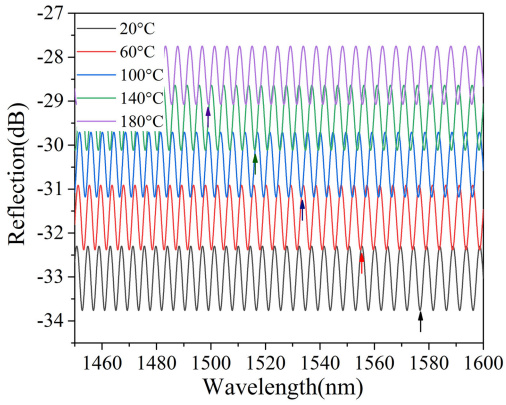

Fig. 3. Simulated reflection spectra of the proposed fiber temperature sensor at different temperature.

condition is satisfied:

$$\lambda_m = \frac{2n_e L}{m} \tag{5}$$

where λ_m is the central wavelength of m_{th} valley. The temperature sensitivity based on the central wavelength shift of the interference valley can be expressed as:

$$\frac{\partial \lambda_m}{\partial T} = \frac{2L}{m}\frac{\partial n_e}{\partial T} = \frac{\lambda_m}{n_e}\beta_{TOC} \tag{6}$$

Assuming $\lambda_m = 1550$ nm, by putting $n_e = 1.361$ and $\beta_{TOC} = -3.7 \times 10^{-4}$ into Eq. (6), the temperature sensitivity can be calculated to be –422 pm/ °C. The interference valley shifts to the shorter wavelength direction as the increasing of the temperature. The mean loss of the interference fringe mainly depends on the first term in Eq. (4). The temperature sensitivity based on the loss variation can be approximatively calculated by:

$$\frac{\partial \xi_{Loss}}{\partial T} = \frac{\partial 10\log_{10}\left[R_1\left(1-B_1\right)\right]}{\partial T} = -\frac{10}{\ln 10}\frac{4n_1}{n_1^2 - n_e^2}\beta_{TOC} \tag{7}$$

By putting $n_1 = 1.452$, $n_e = 1.361$ and $\beta_{TOC} = -3.7 \times 10^{-4}$ into Eq. (7), the temperature sensitivity can be calculated to be 0.037 dBm/ °C. Therefore, the wavelength shift and the mean loss variation of the interference fringe can be both used for temperature sensing synchronously.

4. Experimental Results and Discussion

The fabricated fiber structure with the volume ratio 2.89 of ethanol to air was placed in a tube furnace that was heated from 20 °C to 220 °C with the temperature interval of 10 °C. The target temperature was set through the tube furnace, and the actual temperature was shown on the display screen of the tube furnace. This temperature value came from the thermometer integrated in the tube furnace, and its display resolution was 1 °C. Its reflection spectrum was monitored in real time by using the OSA (AQ6370B) and BBS (1200 nm to 1700 nm) through the circulator. At each temperature, the reflection spectrum was recorded after the temperature had been steady for 5 minutes. The measured reflection spectra at 20 °C, 60 °C, 100 °C, 140 °C and 180 °C are shown in Fig. 4. From Fig. 4 it can be seen that, as the increasing of the temperature, the interference fringe shifted to the shorter wavelength direction. Meanwhile, the mean loss of the interference fringe decreased gradually. The experimental results accord with the simulation results shown in Fig. 3. Then the fiber structure was cooled from 220 °C to 20 °C with the temperature interval of 10 °C. At each temperature, the reflection spectrum was also recorded. Among all the reflection spectrum results, we chose one interference valley and recorded its central wavelength at each temperature

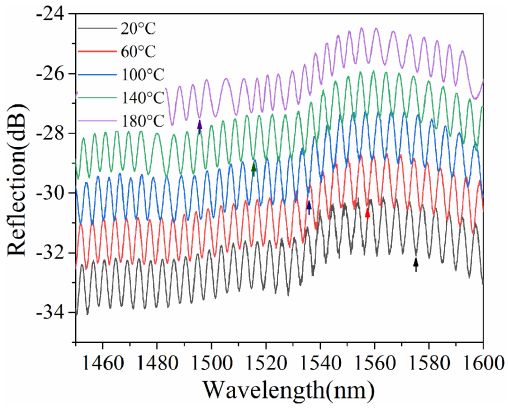

Fig. 4. Measured reflection spectra at 20 °C, 60 °C, 100 °C, 140 °C and 180 °C.

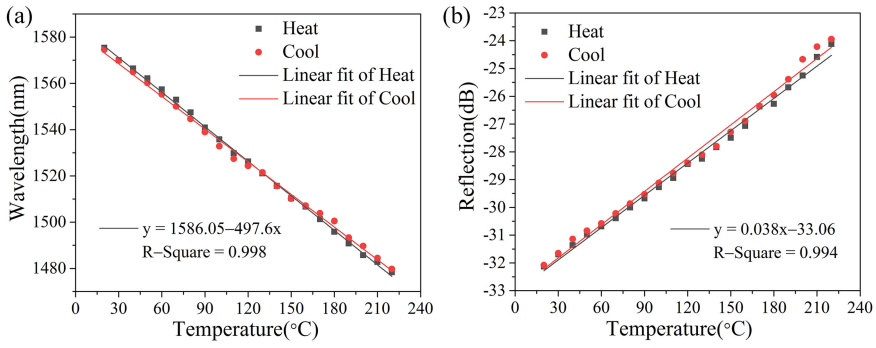

Fig. 5. (a) Relationship between the wavelength shift of the interference fringe and temperature. (b) Relationships between the mean loss of the interference fringe and temperature.

during heating and cooling processes. The central wavelength values and their linear fitting results are shown in Fig. 5(a). The central wavelength shifts of the interference valley have good linear relationships with the temperature variations. The temperature sensitivity based on the wavelength shift of the interference valley reached –497.6 pm/ °C with a linearity of 99.9% between 20 °C and 220 °C. This experimental sensitivity value is in line with theory expectation (–422 pm/ °C). The maximum deviations between the experimental data and the fitting line in heating and cooling processes are 1.75 nm and 3.44 nm respectively, while the average deviations are only 0.82 nm and 1.20 nm respectively. Besides, the fabricated fiber structure also showed a good repeatability in heating and cooling processes. The maximum deviation between the heating and cooling fitting lines is 2.50 nm. Then we calculated the mean loss of the interference fringe in each reflection spectrum by summing the loss values of all the wavelength data points, and the relationships between the mean loss of the interference fringe and temperature in heating and cooling processes are shown in Fig. 5(b). The temperature sensitivity based on the variation of mean loss reached 0.038 dBm/ °C, which is also in line with theory expectation (0.037 dBm/ °C). There is a good linear and repeatable relationship between the mean loss and the temperature. The maximum deviations and average deviations between the experimental data and the fitting are 0.40 dBm and 0.15 dBm (heating process), 0.42 dBm and 0.18 dBm (cooling process), respectively. The maximum deviation between the heating and cooling fitting lines is 0.28 dBm.

What's more, it can be seen in Fig. 4 that the FSR of the interference fringe is only less than 10 nm. Considering the wavelength shift sensitivity of –497.6 pm/ °C, the temperature variation of only 20 °C will make the interference valley shift more than one FSR. As a result, different interference valleys may appear in the same wavelength position at different temperatures. In this

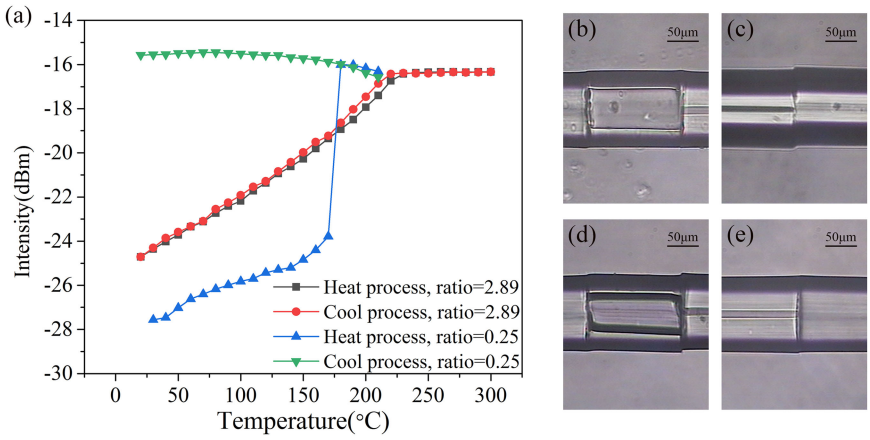

Fig. 6. (a) Power variations of the fabricated two fiber structures with volume ratios of 2.89 and 0.25 respectively in heating and cooling process. (b)-(c) Microscope images of the fiber structure with volume ratio of 0.25 before experiment. (d)-(e) Microscope images of the fiber structure with volume ratio of 0.25 after experiment.

case, we need to distinguish one interference valley from the other when measuring the correct temperature. Otherwise it will result in the failure of the temperature demodulation. This problem can be solved by monitoring the interference valley and the mean loss in the transmission spectrum synchronously for the proposed fiber temperature sensor. In the actual sensing application, the environment temperature can be rough demodulated from the mean loss of interference fringe firstly. Then the position of the chosen interference valley can be predicted. Finally, the environment temperature can be accurately demodulated by measuring the actual central wavelength of the corresponding interference valley. Of course, the proposed fiber sensor can be applied for low-cost and fast-response temperature sensing by using only the power meter and the BBS, for the expensive and cumbersome spectrometer is not necessary any more if the mean loss is only to be monitored.

Then we fabricated another fiber structure with the volume ratio 0.25 of ethanol to air as a contrast. The length of the micro-cavity was about 155 μm. The length of the thin core SCT was about 14148 μm, and a section of air column with a length of about 13960 μm in the thin core SCT was achieved by heating the ethanol in advance before final splicing. The fabricated two fiber structures with the volume ratios 2.89 and 0.25 respectively were both placed in the tube furnace. The tube furnace was heated from 20 °C to 300 °C and then cooled from 300 °C to 20 °C with the temperature interval of 10 °C. Each fiber structure was connected to the BBS (1200 nm to 1700 nm) and a power meter through a circulator. The power variations of the two fiber structures are shown in Fig. 6(a). For the fiber structure with the volume ratio of 2.89, when the temperature increased from 20 °C to 220 °C, the power increased continuously without a sudden change, which means that the ethanol in the fiber structure remained liquid state and expanded gradually. The expansion of the ethanol resulted in the decreasing of its RI. When the temperature reached 220 °C, the whole space in the fiber structure was filled by the liquid ethanol molecules as well as air molecules between them. Then as the further increasing of the temperature, the volume of the liquid ethanol was limited by the sealing space, and the RI of the ethanol changed little. Therefore, the measured power of the fiber structure became stable. When the temperature was higher than the supercritical temperature (about 243 °C) of the ethanol, the intense thermal motions of the ethanol molecules make the ethanol become supercritical state. In the cooling process, the power variations of the fiber structure are consistent with that in the heating process. Therefore, the fabricated fiber structure can work as a sensitive temperature sensor with an upper detection limit of 220 °C. However, for the fiber structure with the volume ratio 0.25 of ethanol to air, when the temperature was increased to 170 °C, the power changed suddenly from −24 dBm to −16 dBm and then became stable,

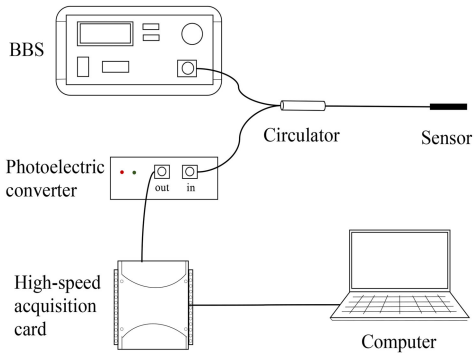

Fig. 7. Experimental setup for temperature cycle experiment.

which means that the ethanol was gasified when the temperature was higher than 170 °C (The boiling point was still higher than 78.3 °C). In the cooling process, the power didn't decease to the initial value. To show the reason, the micro-cavity and thin core SCT of the fiber structure with the volume ratio 0.25 were observed under the microscope before and after the experiment, and the images are shown in Figs. 6(b)–6(e). Comparing Figs. 6(d) and 6(e) to Figs. 6(b) and 6(c) we can see, the gaseous ethanol condensed into liquid when the temperature reached the boiling point in the cooling process. The liquid ethanol flowed into the thin core SCT along the sidewall. Finally, all the liquid ethanol located in the thin core SCT as shown in Fig. 6(e), and the air was left in the micro-cavity formed by the thick core SCT as shown in Fig. 6(d). Therefore, the power of the fiber structure didn't decease even when the temperature was decreased to the room temperature, and the fiber structure can't be used as the temperature sensor any more. The results showed that the fabricated fiber structure with the volume ratio 0.25 can only be expected for temperature sensing with a temperature upper limit lower than 170 °C. Besides, it can also be seen that, if the volume ratio of ethanol to air is not large enough, the proposed sensor will fail to work even at room temperature when the sensor has experienced the temperature higher than its upper detection limit. This problem can be solved when the volume ratio is large enough. The experimental results show that the sensor with the volume ratio of 2.89 can survive the temperature which is higher than its upper detection limit without influencing its sensing performance.

To investigate the repeatability and stability of the proposed fiber temperature sensor with the volume ratio 2.89, we designed a temperature cycle experiment. The temperature of the tube furnace was increased to 220 °C, the proposed fiber sensor was alternately placed in room temperature and 220 °C for nine times. Its light power variation was recorded by using the setup shown in Fig. 7. For the mean loss variation of the interference fringe can also be used for temperature sensing, a BBS (1200 nm to 1700 nm), a photoelectric converter and an acquisition card (sampling frequency was set as 10 Hz) were used to record the sensor response based on the light power variation. The experimental results are shown in Fig. 8. The temperature of the sensor was changed from room temperature to 220 °C immediately in less than 5 s, and the voltage value increased from 0.79 V to 3.35 V correspondingly, which means that the RI of the ethanol in the FP cavity decreased immediately as the increasing of the temperature. After about 30 s, the temperature of the sensor was changed from 220 °C to room temperature again in less than 5 s, and the voltage value also decreased from 3.35 V to 0.79 V correspondingly. This means that the liquid ethanol contracted toward the FP cavity and the RI of the ethanol in the FP cavity increased. More importantly, each time when the sensor was transferred back to the room temperature, the voltage could returned back to the initial value. This is because there is no condensation in the cooling process. For the inner surface area of the FP cavity is much larger than the thin core SCT, the liquid ethanol always contract toward the FP cavity direction each time due to the attraction between the in-wall of the FP cavity and the ethanol molecules. From Fig. 8, it can also be seen that, when the temperature of the tube furnace was kept at 220 °C (shown and controlled by the tube furnace), the voltage

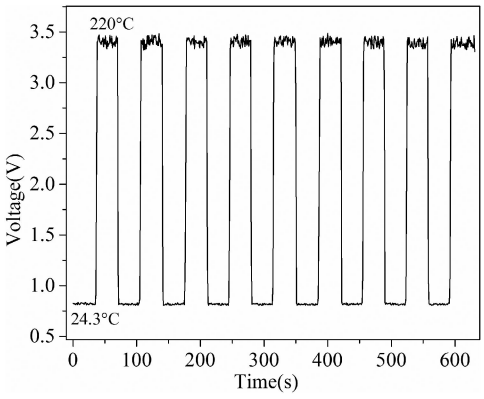

Fig. 8. Light power variations of the sensor during the cycle experiments between room temperature and 220 °C.

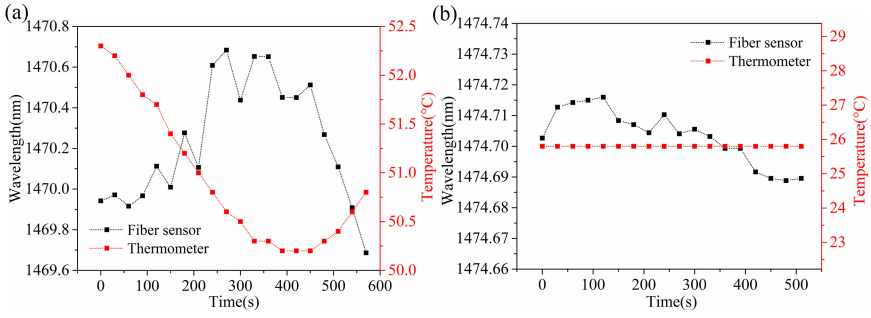

Fig. 9. (a) Central wavelength and temperature fluctuations in the tube furnace. (b) Central wavelength and temperature fluctuations in the insulated cups at room temperature.

fluctuation shown by the sensor is much larger than that in room temperature, which means that the actual temperature in the tube furnace is not stable enough. The large temperature fluctuation of the tube furnace leads to the RI variation of the sealed ethanol in the sensor, which influences the power loss of the sensor and results in the large noise of the voltage values.

To show the temperature fluctuation of the tube furnace, the thermometer (resolution 0.1 °C) together with the fabricated fiber sensor was placed in the tube furnace. When the tube furnace reached the target temperature, the values of the thermometer and the central wavelength values of the fiber sensor were recorded synchronously for 10 minutes with the interval of 30 s. The results are shown in Fig. 9(a). From Fig. 9(a), the thermometer values show that temperature fluctuation in the tube furnace is about 2.1 °C. Meanwhile, the central wavelength variation of the fabricated fiber sensor in the same environment is about 0.997 nm. Therefore, the different slopes and deviation of some temperature points as shown in Fig. 5 may be mainly induced by the temperature fluctuation of the tube furnace. To achieve an environment with more stable temperature, the thermometer and the fiber sensor were kept together in an insulated cup in room temperature. Their values were also recorded for 10 minutes, and the results are shown in Fig. 9(b). The thermometer remained 25.8 °C during the 10 minutes, and the central wavelength variation of the sensor was only 0.025 nm.

The response time of the fabricated temperature sensor was measured also by using the setup shown in Fig. 7. Two insulated cups contained the ice water and boiling water respectively, and two thermometers with a resolution of 0.1 °C were kept individually in the cups to show the temperature in real time. The sensor was placed in these two cups in turn. The light power variations of the sensor in the whole process are recorded as the voltage values through the photoelectric converter continuously. The results are shown in Fig. 10(a). From Fig. 10(a) it can be seen that, at each

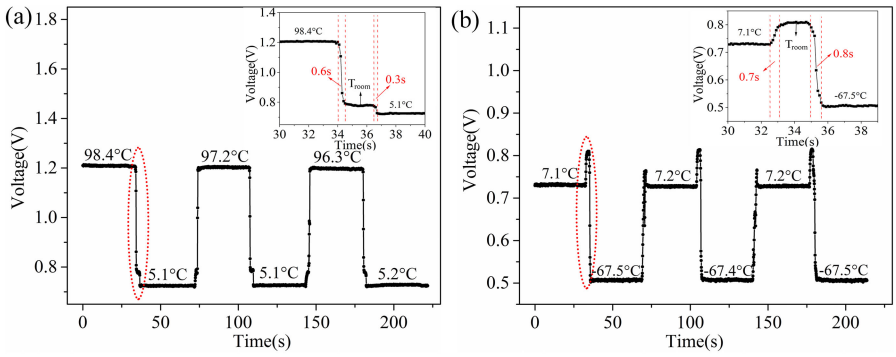

Fig. 10. Light power variations of the sensor during the cycle experiments.

temperature environment, the voltage values remain stable. When the temperature is 98.4 °C and 5.1 °C, the mean values of the voltages are 1.21 V and 0.72 V, and the standard deviations of the voltages are 0.0019 V and 0.0013 V, respectively. When the sensor was transferred from 98.4 °C to 5.1 °C, the voltage value decreased from 1.21 V to 0.72 V after about 2.5 s, which was the time that we took to transfer the sensor. In this process, for sensor was transferred from 98.4 °C to 5.1 °C through room temperature, the voltage value was decreased to about 0.78 V firstly and then was stable for a while, which means the room temperature was also shown by the sensor. Therefore the response time of the sensor from 98.4 °C to room temperature is about 0.6 s. When the sensor was transferred from 5.1 °C to 97.2 °C, the voltage value increased from 0.72 V back to 1.21 V, and room temperature was also shown. Then a plastic cup containing the ethanol was placed in a dry ice bath as a sub-zero temperature environment (−67.5 °C shown by the thermometer). The whole step was insulated. The sensor was alternately placed in 7.1 °C and −67.5 °C. The recorded voltage values are shown in Fig. 10(b). When the temperature is 7.1 °C and −67.5 °C, the mean values of the voltages are 0.73 V and 0.51 V, and the standard deviations of the voltages are 0.0013 V and 0.0015 V, respectively. From Fig. 10(b) it can be seen that, when the sensor was transferred from 7.1 °C to −67.5 °C through the room temperature, the voltage value increased from 0.73 V to 0.81 V firstly, and then decreased to 0.51 V. The response time of the sensor from room temperature to − 67.5 °C is about 0.8 s.

From Fig. 8 and Fig. 10, it can also be seen that, during the repeating temperature increasing and decreasing processes, the voltage always returned to the same value each time in the same temperature environment. Therefore, the proposed sensor exhibited good repeatability and stability, and there was no obvious relevant hysteresis in the cycle experiments. Instead, the sensor showed fast temperature response. Besides, for the inner diameter of the thin core SCT was only 13 μm, the ethanol column was stuck in the thin core SCT due to the capillary force. The slope and vibration of the sensor cannot transfer the air column left in the thin core SCT to the ethanol micro-cavity through the ethanol column, which can be confirmed in our experiments. Therefore, the influence of slope and vibration on the sensor performance can also be ignored.

5. Conclusion

We proposed a highly-sensitive and fast-responsive optical fiber temperature sensor based on the sealed liquid ethanol with a large detection range (up to 220 °C). The sealed ethanol can remain liquid state as the increasing of the temperature until its supercritical temperature (about 243 °C) at which the ethanol becomes supercritical state. The wavelength shift and mean loss variation of the interference fringe can both be used for temperature sensing with the sensitivities of –497.6 pm/ °C and 0.038 dBm/ °C respectively. The response time is less than 1 s for the large temperature variation of about 90 °C. Therefore, the proposed optical fiber temperature sensor may

find widespread application owing to its high sensitivity, good linearity, large detection range, fast response, good repeatability and stability.

References

[1] Y. H. Zhang and W. Y. Yang, "Simultaneous precision measurement of high temperature and large strain based on twisted FBG considering nonlinearity and uncertainty," *Sensors Actuators A: Physical*, vol. 239, pp. 185–195, 2016.
[2] T. T. Yuan *et al.*, "Long period fiber grating in two-core hollow eccentric fiber," *Opt. Exp.*, vol. 23, no. 26, pp. 33378–33385, 2015.
[3] Z. Y. Zhao *et al.*, "All-solid multi-core fiber-based multipath Mach–Zehnder interferometer for temperature sensing," *Appl. Phy. B.*, vol. 112, pp. 491–497, 2013.
[4] J. M. Hsu, W. H. Zheng, J. Z. Chen, C. L. Lee, and J. S. Horng, "Temperature fiber sensors based on Mach–Zehnder interferometer with sturdy structure," *IEEE Sensors J.*, vol. 15, no. 12, pp. 6995–7000, Dec. 2015.
[5] J. J. Wang, B. Dong, E Lally, J. M. Gong, M. Han, and A. B. Wang, "Multiplexed high temperature sensing with sapphire fiber air gap-based extrinsic Fabry–Perot interferometers," *Opt. Lett.*, vol. 35, no. 5, pp. 619–621, 2010.
[6] T. Zhu, T. Ke, Y. J. Rao, and K. S. Chiang, "Fabry–Perot optical fiber tip sensor for high temperature measurement," *Opt. Commun.*, vol. 283, pp. 3683–3685, 2010.
[7] Y. Mohanna, J. M. Saugrain, J. C. Rousseau, and P. Ledoux, "Relaxation of internal stresses in optical fibers," *J. Lightw. Technol.*, vol. 8, no. 12, pp. 1799–1802, 1990.
[8] Y. Q. Li, F. C. Zhang, and T. Yoshino, "Wide-Range temperature dependence of Brillouin shift in a dispersion-shifted fiber and its annealing effect," *J. Lightw. Technol.*, vol. 21, no. 7, pp. 1663–1667, Jul. 2003.
[9] U. Sampath, D. G. Kim, H. Kim, and M. Song, "Cryogenic temperature sensor based on Fresnel reflection from a polymer-coated facet of optical fiber," *IEEE Sensors J.*, vol. 18, no. 9, pp. 3640–3644, May 2018.
[10] R. Rinaudo, I. Paya-Zaforteza, P. Calderón, and S. Sales, "Experimental and analytical evaluation of the response time of high temperature fiber optic sensors," *Sensors Actuators A: Physical*, vol. 243, pp. 167–174, 2016.
[11] Y. Xue *et al.*, "Ultrasensitive temperature sensor based on an isopropanol-sealed optical microfiber taper," *Opt. Lett.*, vol. 38, no. 8, pp. 1209–1211, 2013.
[12] A. Zhou, Y. X. Zhang, Q. Xu, J. Yang, and L. B. Yuan, "Semi-open cavity in-fiber Mach–Zehnder interferometer for temperature measurement with ultra-high sensitivity," *Appl. Opt.*, vol. 53, no. 12, pp. 2696–2701, 2014.
[13] D. J. J. Hu *et al.*, "Fabrication and characterization of a highly temperature sensitive device based on nematic liquid crystal-filled photonic crystal fiber," *IEEE Photon. J.*, vol. 4, no. 5, pp. 1248–1255, Oct. 2012.
[14] X. C. Yang, Y. Lu, B. L. Liu, and J. Q. Yao, "Fiber ring laser temperature sensor based on liquid-filled photonic crystal fiber," *IEEE Sensors J.*, vol. 17, no. 21, pp. 6948–6952, Nov. 2017.
[15] L. Cheng *et al.*, "Ultrahigh temperature sensitivity using photonic bandgap effect in liquid-filled photonic crystal fibers," *IEEE Photon. J.*, vol. 9, no. 3, Jun. 2017, Art. no. 6802907.
[16] Y. Q. Yu *et al.*, "Some features of the photonic crystal fiber temperature sensor with liquid ethanol filling," *Opt. Exp.*, vol. 18, no. 15, pp. 15383–15388, 2010.
[17] Y. Xin, X. Y. Dong, Q. Q. Meng, F. Qi, and C. L. Zhao, "Alcohol-filled side-hole fiber Sagnac interferometer for temperature measurement," *Sensors Actuators A: Physical*, vol. 193, pp. 182–185, 2013.
[18] M. Li, Y. Liu, R. X. Gao, Y. Li, X. L. Zhao, and S. L. Qu, "Ultracompact fiber sensor tip based on liquid polymer-filled Fabry-Perot cavity with high temperature sensitivity," *Sensors Actuators B: Chem.*, vol. 233, pp. 496–501, 2016.
[19] S. J. Weng, L. Pei, J. S. Wang, T. G. Ning, and J. Li, "High sensitivity D-shaped hole fiber temperature sensor based on surface plasmon resonance with liquid filling," *Photon. Res.*, vol. 5, no. 2, pp. 103–107, 2017.
[20] X. C. Yang, Y. Lu, B. L. Liu, and J. Q. Yao, "High sensitivity hollow fiber temperature sensor based on surface plasmon resonance and liquid filling," *IEEE Photon. J.*, vol. 10, no. 2, Apr. 2018, Art. no. 6801909.
[21] W. W. Qian *et al.*, "Temperature sensing based on ethanol-filled photonic crystal fiber modal interferometer," *IEEE Sensors J.*, vol. 12, no. 8, pp. 2593–2597, Aug. 2012.
[22] S. H. Liu, Y. Wang, M. X. Hou, J. T. Guo, Z. H. Li, and P. X. Lu, "Anti-resonant reflecting guidance in alcohol-filled hollow core photonic crystal fiber for sensing app lications," *Opt. Exp.*, vol. 21, no. 25, pp. 31690–31697, 2013.
[23] W. W. Qian *et al.*, "High-sensitivity temperature sensor based on an alcohol-filled photonic crystal fiber loop mirror," *Opt. Lett.*, vol. 36, no. 9, pp. 1548–1550, 2011.
[24] C. L. Zhao *et al.*, "Phenomenon in an alcohol not full-filled temperature sensor based on an optical fiber Sagnac interferometer," *Opt. Lett.*, vol. 37, no. 22, pp. 4789–4791, 2012.
[25] D. Wu, Y. Zhao, and H. F. Hu, "Experimental research on FLM temperature sensor with an ethanol-filled photonic crystal fiber," *Sensors Actuators A: Physical*, vol. 209, pp. 62–67, 2014.
[26] B. Dong, Z. Y. Shen, C. Y. Yu, and Y. X. Wang, "Modal excitations in fully and partially ethanol-filled photonic bandgap fibers and their applications as fiber sensors," *J. Lightw. Technol.*, vol. 34, no. 16, pp. 3853–3858, Aug. 2016.
[27] F. Q. Shi, Y. Y. Luo, D. R. Chen, J. J. Chen, Z. J. Ren, and B. J. Peng, "A dual-parameter sensor based on the asymmetry of alcohol filling the photonic crystal fiber in sagnac loop," *IEEE Sensors J.*, vol. 18, no. 15, pp. 6188–6195, Aug. 2018.
[28] Y. Mao, Y. X. Zhang, R. K. Xue, Y. Liu, K. J. Cao, and S. L. Qu, "Compact optical fiber temperature sensor with high sensitivity based on liquid-filled silica capillary tube," *Appl. Opt.*, vol. 57, no. 5, pp. 1061–1066, 2018.
[29] Z. L. Ran, Y. J. Rao, W. J. Liu, X. Liao, and K. S. Chiang, "Laser-micromachined Fabry-Perot optical fiber tip sensor for high-resolution temperature independent measurement of refractive index," *Opt. Exp.*, vol. 16, no. 3, 2252–2263, 2007.
[30] C. L. Lee, H. Y. Ho, J. H. Gu, T. Y. Yeh, and C. H. Tseng, "Dual hollow core fiber-based Fabry-Perot interferometer for measuring the thermo-optic coefficients of liquids," *Opt. Lett.*, vol. 40, no. 4, pp. 459–462, 2015.